Transition Metal Chemistry
https://doi.org/10.1007/s11243-024-00584-9

N-doped TiO_2 for photocatalytic degradation of colorless and colored organic pollutants under visible light irradiation

Abdul Wafi[1,2] · Liszulfah Roza[3] · Gerald Ensang Timuda[3] · Demas Aji[1] · Deni Shidqi Khaerudini[1] · Nono Darsono[4] · Nurfina Yudasari[5] · Erzsébet Szabó-Bárdos[6] · Ottó Horváth[6] · Mohammad Mansoob Khan[7]

Received: 19 March 2024 / Accepted: 21 April 2024

Abstract
Titanium dioxide (TiO_2) can only be stimulated by UV light, making its real application for photocatalytic water treatments ineffective, particularly under sunlight and visible light irradiation. As a result, significant efforts have been conducted over the last decades to fabricate visible light-active TiO_2 photocatalysts through band-gap engineering. Herein, nitrogen-doped titanium dioxide (N-TiO_2) photocatalysts were effectively prepared by utilizing a simple sol–gel process with ethanol as a single solvent and urea as the nitrogen source under ambient temperature and pressure. The effects of urea concentration (0, 2, 4, 6 urea/TTIP mol ratio) on the optical, structural, morphological, and photocatalytic properties of the photocatalysts were investigated. SEM morphology revealed an aggregated nano-spherical shape in all samples. HR-TEM and SAED patterns showed an anatase phase of 2-N-TiO_2. The X-ray diffraction analysis also showed a pure anatase phase for pure TiO_2, 2-N-TiO_2, and 4-N-TiO_2. However, the crystalline phase transformed to amorphous for 6-N-TiO_2. The crystallite size reduced from 14.16 to 9.76 nm upon increasing urea concentration. The band-gap energy of N-TiO_2 also decreased from 3.25 to 2.95 eV. Furthermore, the photocatalytic experiment was examined for the degradation of colorless and colored pollutants, such as salicylic acid (SA), methyl blue (MB), and rhodamine B (RhB). The results showed the photocatalytic activity of 2-N-TiO_2 exhibited an optimum efficiency compared to the 4-N-TiO_2 and 6-N-TiO_2, for photocatalytic degradation of SA ($k = 0.0265\ min^{-1}$), MB ($k = 0.0180\ min^{-1}$) and RhB ($k = 0.1071\ min^{-1}$), under visible light irradiation. Therefore, the results suggest that crystallite size, urea (as an N dopant) concentration, and organic model pollutants were critical parameters for the photocatalytic activity of N-TiO_2 under visible irradiation.

Introduction

The growing number of ecologically hazardous substances requires the development of innovative processes that can be successfully applied to an extensive range of pollutants. This condition can be satisfied by heterogeneous photocatalysis because it can produce reactive oxygen species (ROS) to decompose and mineralize organic pollutants, such as pharmaceuticals, dyes, surfactants, pesticides, etc. [1, 2].

Among the heterogeneous photocatalysts, TiO_2 is a photoactive catalyst that is commonly employed in this application, due to its distinctive qualities, including high chemical stability, low cost, non-toxicity, and strong optical activity [3–5]. However, several problems with TiO_2 continue to restrict its real application. For instance, TiO_2 could only be activated under ultraviolet (UV) irradiation and could not be efficiently employed under sunlight or visible light due to its wide band-gap energy (3.2 eV) [6, 7].

To solve the problem, nitrogen doping has shown an effective strategy to shift the TiO_2 absorption into the visible spectrum. Nitrogen can introduce a new energy level between the conduction and valence band of the TiO_2, leading to band-gap narrowing [8–10].

The synthesis approach plays an important role to producing better material properties and photocatalytic activity [11]. Several techniques have been used to prepare N-TiO_2, including electrophoretic depositional (EPD) [12], vapor deposition, hydrothermal [13], co-precipitation [14], and sol–gel [15].

Based on our previous study, several parameters such as synthesis method, nitrogen source, and calcination temperature could be crucial features to improve the N-TiO_2 characteristics and photocatalytic activity [16]. Porous and non-porous were obtained by different synthesis methods which were affecting the specific surface area and photocatalytic

Extended author information available on the last page of the article

Published online: 14 May 2024

activity. In addition, the crystallite size could be improved by increasing the calcination temperature. However, the nitrogen content evaporated at high calcination temperatures and reduced the photocatalytic activity [16, 17]. Therefore, we were greatly interested in continuing the study by investigating the effect of nitrogen intake during the N-TiO_2 preparation on the material characteristic and on the photoactivities, which was not reported in our previous research [16].

In 2023, Khan and his fellow workers synthesized N-TiO_2 photocatalyst using triethylamine as a nitrogen source. Other organic solvents such as Tween 80, acetic acid, and iso-propanol were used during the preparation. No triethylamine optimization (concentration) was observed in the report. The photocatalytic activity of the prepared N-TiO_2 showed significant degradation of 2,4-dichlorophenol under visible irradiation for 240 min. The degradation percentage of 2,4-dichlorophenol over N-TiO_2 was 77.6% which was higher than control TiO_2 with the value of 21.5% [18]. In addition, Mahendrasingh, et al., also reported an effect of nitric acid concentration (2–6 mol%) as a nitrogen source to prepare N-TiO_2 photocatalyst. Various solvents were added during the synthesis process, including ethanol, 1, 3-diaminopropane, and ethylene glycol. The photocatalytic activity showed that optimum photo-decomposition of methylene blue over N-TiO_2 was found at 2 mol% of nitrogen dopant with removal of 94.5% within 100 min under visible irradiation [19].

In the present work, another nitrogen source, urea (as an N dopant) has been used to prepare a N-TiO_2 photocatalyst via modified sol–gel under ambient temperature and pressure. A single and eco-friendly solvent like ethanol was used in the present study to minimize the environmental effect during the preparation. Ethanol is a universal solvent in chemical synthesis and can be easily evaporated after the synthesis process. Therefore, the modified sol–gel method used in this study is promising for practical application because of its inexpensive, simple, and easy to operate under ambient temperature and pressure. In addition, the effect of urea intake on the material's properties including morphology, vibration, crystalline structure, band-gap energy, and surface area was examined and discussed in detail. Furthermore, different characteristics of organic pollutants from colorless and colored groups such as SA (drug), MB (dye), and RhB (dye) were utilized to examine the photocatalytic degradation efficiency of N-TiO_2 under visible light irradiation. SA is colorless and a simple phenolic compound commonly used as an anti-inflammatory drug in the medical and pharmaceutical industries [20]. However, MB and RhB are artificial colors widely used in several industries, such as dyeing in textiles, printing, paint, leathers, papers, etc. [21]. Therefore, the removal of these organic pollutants is still a great challenge and critical to control and minimize their environmental risks in the future.

Materials and methods

Materials

All the chemicals used in this experiment were analytical grade including titanium (IV) iso-propoxide, TTIP ($Ti[OCH(CH_3)_2]_4$) 98% was obtained from Sigma-Aldrich. Urea (CH_4N_2O), Ethanol 70%, salicylic acid (SA, $C_7H_6O_3$), methyl blue (MB, $C_{37}H_{27}N_3Na_2O_9S_3$), and rhodamine B (RhB, $C_{28}H_{31}ClN_2O_3$) were obtained from Merck. The distilled water used in all experiments was obtained from a Milli-Q water purification.

Preparation of nano-spherical N-TiO_2

The nano-spherical N-TiO_2 was prepared by using the previous method with some modifications [22]. Typically, 5 mL of TTIP was dissolved in 40 mL of ethanol. Then, various amounts (0, 2, 4, and 6 urea/TTIP mol ratio) of urea in 10 mL of distilled water were slowly added into the TTIP solution and homogeneously stirred at room temperature for 60 min. Subsequently, a white suspension was evaporated and dried in the oven at 80 °C for 15 h. The white precipitate obtained was calcined at 450 °C for 30 min in an air atmosphere with a heating rate of 5 °C min^{-1}. The prepared catalysts are coded as x-N-TiO_2, where x ($x = 0, 2, 4, 6$) represents the urea/TTIP mol ratio. For comparison, pure TiO_2 was also prepared in a similar manner without urea addition. The obtained catalysts (Figure S1) then were subjected to characterization and photocatalytic experiments.

Material characterization

The as-prepared photocatalysts were characterized in a physicochemical manner using various equipment. The vibration characteristics of the photocatalysts were measured by using FTIR-ATR Thermo Scientific Nicolet iS, (Fourier transform infrared spectroscopy-attenuated total reflection). The morphology and elemental analysis were measured by Scanning Electron Microscope (SEM, Hitachi SU3500) and energy-dispersive X-ray (EDX, Hitachi SU3500). The High-resolution Transmission Electron Microscope (HR-TEM) and the Selected Area Diffraction pattern (SAED) were measured using the Tecnai G2 20 S-TWIN Transmission Electron Microscope. The crystal structure and phase purity were examined by X-ray diffraction (XRD, Rigaku SmartLab). The optical properties were measured by UV–Vis diffuse reflectance spectrophotometer (DRS, Ocean Optic Inc.). The specific surface area was determined by nitrogen adsorption–desorption isotherms measured with a Quantachrome Nova 4200e instrument. The photocatalytic experiment was

examined under visible light irradiation using 3 Phillips lamps (3 × 18 W) as light sources. Then, the absorbance of organic pollutants was measured using an UV–Vis spectrophotometer (Thermo Scientific Genesys 10S).

Photocatalytic experiment

The photocatalytic activity of nano-spherical N-TiO_2 samples was examined through the photocatalytic degradation of various model organic pollutants, such as SA, MB, and RhB. A rectangular black box consisting of 3 visible lamps (3 × 18 W) was used as a lab-scale photocatalytic reactor as illustrated in Fig. 1.

Initially, 20 mg of N-TiO_2 samples were added into 20 mL of 10 µM model pollutant aqueous solution and homogeneously stirred for 30 min. The suspension was placed in a black box and continuously left in the dark for 30 min for adsorption–desorption to achieve an equilibrium. Then the fluorescent lamps inside the black box were turned on to start the photocatalytic reaction. After given time intervals, 2 mL of suspension was taken and separated through centrifugation at 400 rpm for 3 min. Then, an UV–Vis spectrophotometer was used to measure the absorbance of the actual pollutant concentration. The intermediates or end products could not be detected by using this measurement. Equation 1 was used to determine the photocatalytic degradation efficiency ($D(t)$, %).

$$D(t)(\%) = \frac{A_0 - A_t}{A_0} \times 100 \quad (1)$$

where A_0 is the initial and A_t is the actual absorbance of the pollutants [23–25].

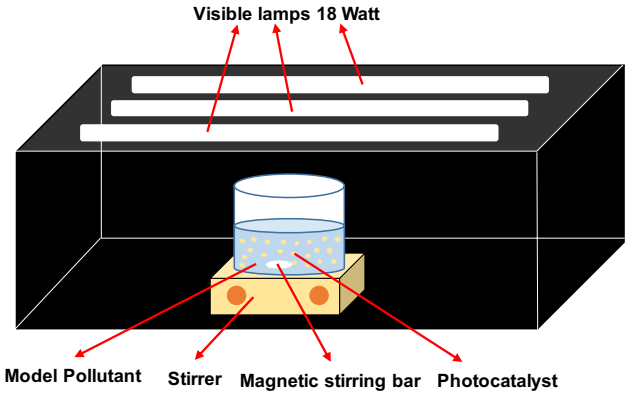

Fig. 1 Illustration of the black box for photocatalytic reactor. (Color figure online)

Result and discussion

Material properties

The FTIR spectrum of the prepared photocatalysts is shown in Fig. 2a. Generally, the FTIR spectra of both pure TiO_2 and N-TiO_2 are similar. A broad peak from 500 to 1000 cm^{-1} could be assigned to the stretching of Ti–O and Ti–O–Ti bonds [26]. Another broad peak around 3000 to 3500 cm^{-1} was attributed to the O–H stretching [27], and O–H bending was indicated by a peak at 1621 cm^{-1} [28]. However, in the case of nitrogen doping, two characteristic peaks located

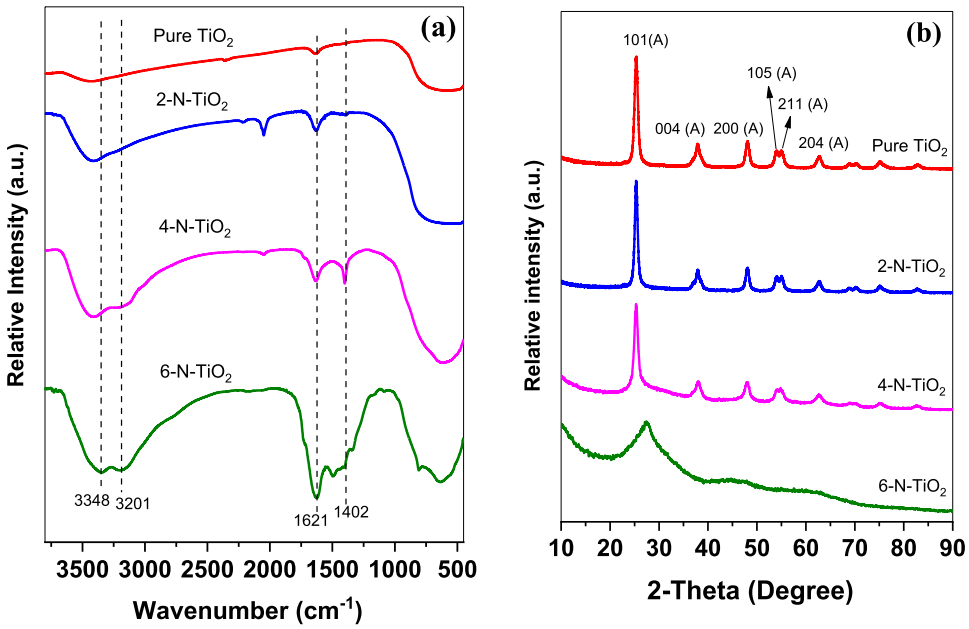

Fig. 2 **a** FTIR spectra and **b** XRD patterns of the prepared photocatalysts

at 3201 and 3348 cm^{-1} appeared which were more intense as the nitrogen concentration increased. Those peaks, even though overlapped with the O–H band, can be assigned to the N–H stretching [14, 17]. Another characteristic peak for N-TiO_2 was revealed at 1402 cm^{-1}, designated to the N–H bending [29] which indicates the incorporation of N into the TiO_2 lattice [14].

Figure 2b represents the XRD patterns of pure TiO_2 and N-TiO_2. All the photocatalysts are well-crystalline materials except 6-N-TiO_2. All peaks of N-TiO_2 are slightly broader than the peaks of pure TiO_2 due to the substitution of the N atom into the TiO_2 structure. The crystalline structure was dominated by the anatase phase for pure TiO_2 and it remained unchanged after nitrogen doping (2-N-TiO_2 and 4-N-TiO_2). However, at higher urea concentration (6-N-TiO_2), the sample seems to be transformed into an amorphous phase. It might be due to all N dopants were not able to enter the TiO_2 lattice during the synthesis and some of the dopants remained on the surface of TiO_2 or their grain boundaries. As a consequence, the surface defect of TiO_2 increased and then prevented the formation of TiO_2 crystals [19].

Table 1 Crystallinity properties and band-gap energy of the prepared photocatalysts

Catalyst	Crystalline phase	Crystallite size (nm)	Band-gap energy (eV)
Pure TiO_2	Anatase	14.16	3.25
2-N-TiO_2	Anatase	13.83	3.14
4-N-TiO_2	Anatase	9.76	3.07
6-N-TiO_2	Amorphous	N/A	2.95

The Scherrer equation was used to determine the crystallite sizes of the photocatalysts. Pure TiO_2, revealed the highest crystallite size of 14.16 nm. Its value gradually decreased with the increase of N doping as shown in Table 1. This suggests that N doping into the TiO_2 lattice could interfere with the crystal growth process of TiO_2 and lower the crystallite size [19]. Crystal growth in amorphous material may be explained as a type of boundary migration from the nucleus surface to the outside. When N atoms come into touch with the boundaries, they can be separated. Then, the separated N atoms can inhibit the crystal grain formation. Therefore, the crystallite size of N-TiO_2 is smaller than that of pure TiO_2 [30].

Furthermore, optical characteristics were examined by using UV–vis diffuse reflectance spectroscopy. Figure 3a represents the diffuse reflectance spectra of the prepared photocatalysts. Compared to pure TiO_2, the absorption edge moved to a larger wavelength after N doping. It can be assigned to the charge-transfer transition between the d–electrons of the dopant and the conduction band of TiO_2 [31].

Furthermore, the band-gap energies of the photocatalysts were calculated using the Kubelka–Munk function as shown in Fig. 3b. Generally, following N doping, the band-gap energy of pure TiO_2 decreased partially. This might be because N has substituted O in the TiO_2 structure, which had different binding characteristics [32, 33], resulting in a narrowing of the band-gap. As a consequence, the TiO_2 absorption moved toward the higher wavelengths, i.e. a red shift has been observed [14, 34]. The current finding is completely consistent with earlier publications that reported band-gap energies of N-TiO_2 samples ranging from 2.94 to 3.18 eV. [11, 13–16]. Table 1 shows the bandgap energies of the prepared photocatalysts.

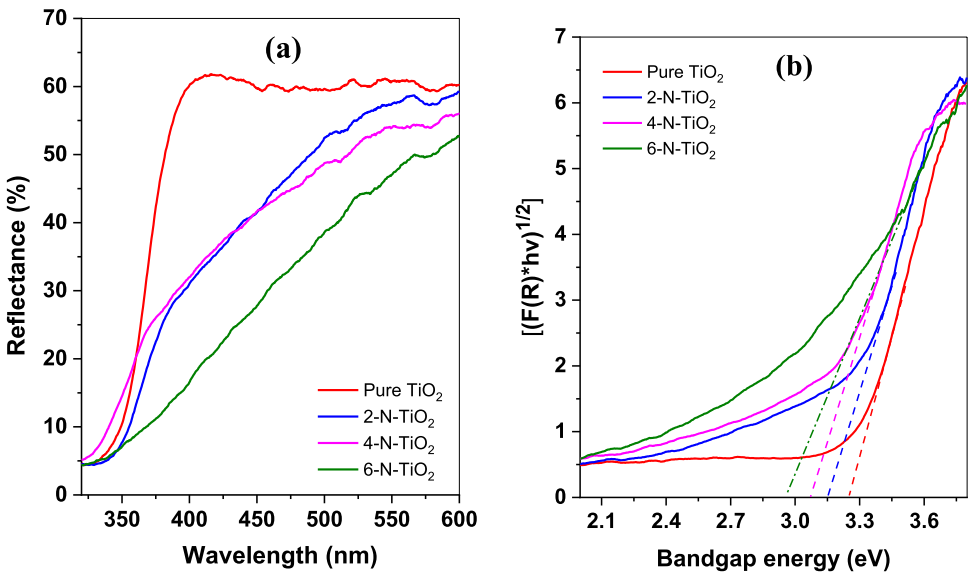

Fig. 3 **a** Diffuse reflectance and **b** Tauc plots constructed from Kubelka–Munk transformed diffuse reflectance spectra for prepared photocatalysts

SEM morphology revealed that all prepared catalysts have spherical shape nanoparticles with an agglomeration (Fig. 4). The average spherical diameter of pure TiO_2, 2-N-TiO_2, and 4-N-TiO_2 were similar with approximately 280–400 nm. However, the diameter of 6-N-TiO_2 became bigger with an average of 350–650 nm (Fig. 5). This observation suggests that more defects and aggregates were possibly formed when doped with a higher concentration of nitrogen [11]. The excessive effect of the nitrogen dopant of the 6-N-TiO_2 can also be observed from the EDX measurement. Nitrogen content was detected only in the case of the 6-N-TiO_2 sample with an atomic percentage of 1.78% (Fig. 6). The N content for pure TiO_2, 2-N-TiO_2, and 4-N-TiO_2 could not be detected (Figure S2–S4), probably due to the sensitivity limit of the EDX device, indicating the non-existent of N atom for pure TiO_2, and a very small amount of N atom infiltrating the crystal structure of TiO_2 for 2-N-TiO_2 and 4-N-TiO_2.

Moreover, the spherical shape materials with an agglomeration of 2-N-TiO_2 photocatalyst were also obtained from TEM measurement (Fig. 7a and b), which is in accordance with SEM results. In addition, the HR-TEM image reveals the d-spacing between the two is around 3.45 Å, which is corresponds to the (101) crystal plane of TiO_2 (Fig. 7c) [35]. The result is also supported by typical concentric rings in the selected area diffraction pattern (SAED), which are consisting crystal planes of (101), (004), (200), (211), (204), indicating the presence of anatase phase in the sample (Fig. 7d). The SAED result was also in agreement with XRD patterns previously discussed in Fig. 2b [36].

Furthermore, the specific surface area of a particle is known to be a function of porosity and pore size distribution which is crucial in material characterization [11]. The nitrogen adsorption–desorption isotherms for the pure TiO_2 and N-TiO_2 samples are shown in Fig. 8. The result shows a mesoporous structure [37, 38] and a typical type IV isotherm according to the Brunauer-Deming-Deming-Teller (BDDT) classification. According to IUPAC, the relative pressure (P/P_0) between 0.8 and 1.0 of the hysteresis loops indicates the presence of mesoporous structure (2–50 nm) [39, 40]. This result is also confirmed by the XRD results in which the calculated crystallite size of the samples was less than 50 nm as shown in Table 1.

The hysteresis type of pure TiO_2 and 2-N-TiO_2 were classified into H4 hysteresis according to IUPAC, which demonstrates a complex material having both micropores and

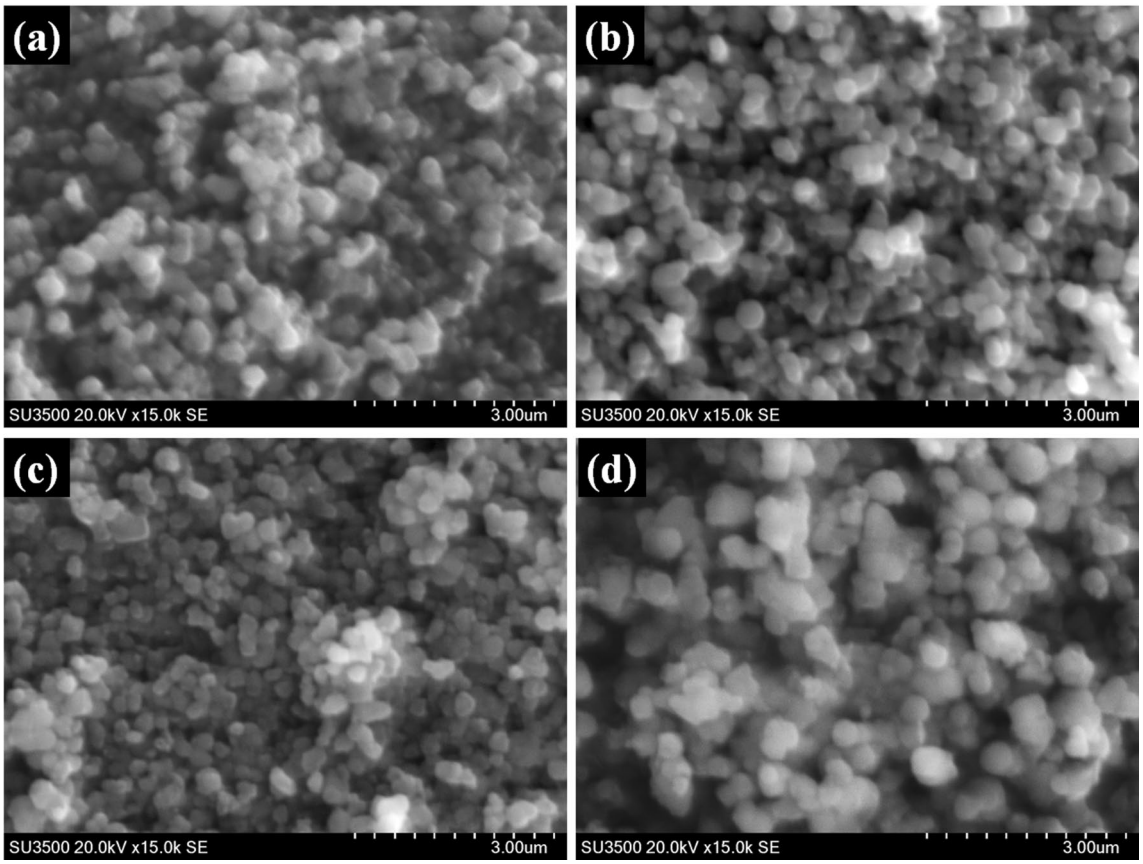

Fig. 4 SEM images of **a** pure TiO_2, **b** 2-N-TiO_2, **c** 4-N-TiO_2, and **d** 6-N-TiO_2

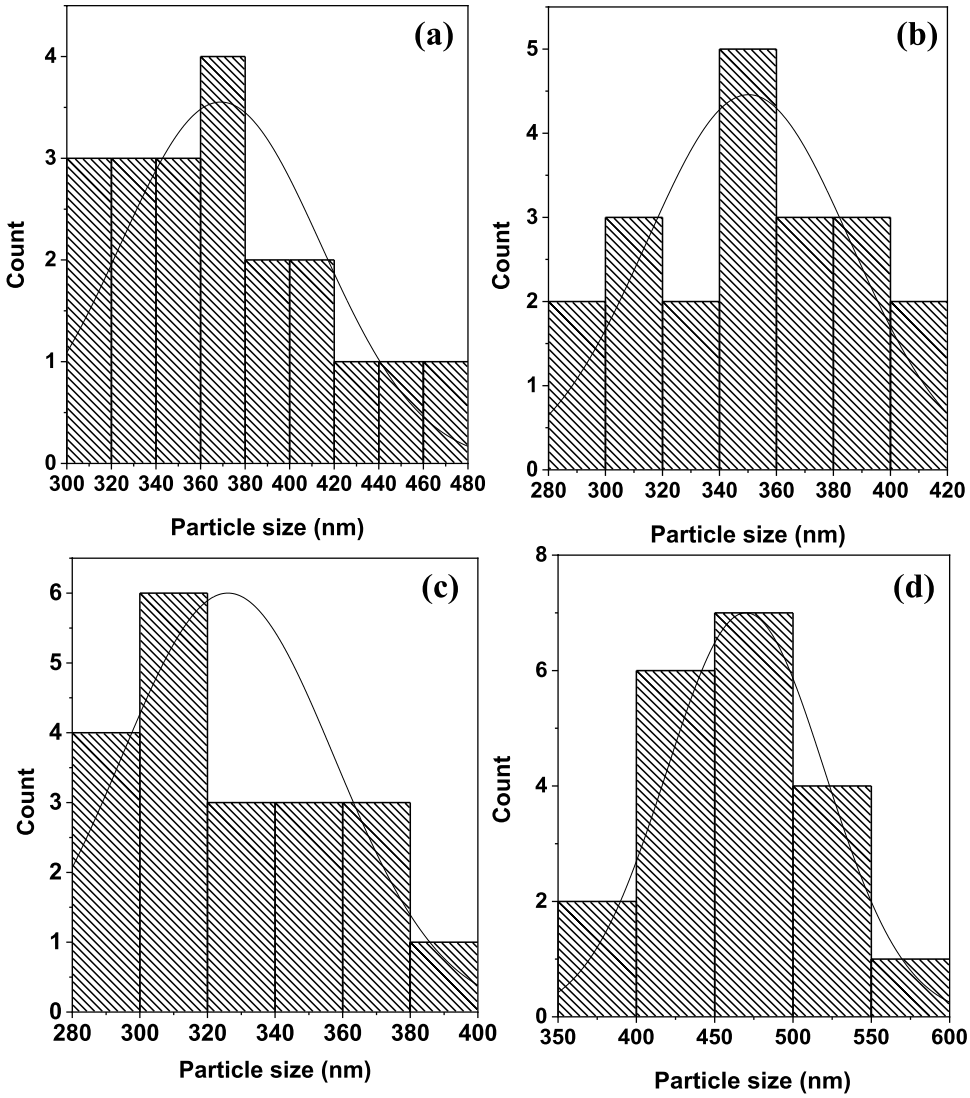

Fig. 5 Particle size distribution of **a** pure TiO_2, **b** 2-N-TiO_2, **c** 4-N-TiO_2, and **d** 6-N-TiO_2

mesopores [41]. Interestingly, at a higher urea concentration (6-N-TiO_2), the hysteresis loop changed into H3 type which indicates that the existence of a non-rigid particle aggregate prevents adsorption at a high relative pressure (P/P_0) [41]. In addition, the hysteresis loop shifted to the left direction (lower relative pressure) resulting in a smaller area of hysteresis for pure TiO_2, 2-N-TiO_2, and 6-N-TiO_2. This phenomenon indicates that the average pore size and pore volume decreased in the presence of N dopant [13]. Then, the BJH model of desorption nitrogen isotherm was used to determine the average pore size and volume as illustrated in Table 2. The results show that average pore size and volume became smaller when pure TiO_2 was doped by nitrogen, which is in accordance with the hysteresis loop model of the present work.

Furthermore, the multi-point BET approach was used to determine the specific surface area as shown in Table 2. The results indicate that pure TiO_2 possesses the highest surface area of 95.907 m^2/g, followed by 2-N-TiO_2 and 6-N-TiO_2 with a value of 67.841 and 63.743 m^2/g, respectively. A smaller surface area typically indicates that the particle size is larger. However, the average particle size between pure TiO_2 and 2-N-TiO_2 observed from SEM measurement was about the same. Furthermore, the average pore volume and diameter were smaller as the surface area was smaller. These indicate the presence of aggregation after nitrogen doping [19]. Suwannaruang and coworkers prepared nano-rice N-TiO_2 via the hydrothermal method and used various urea concentrations (1–12.5% N) as nitrogen sources [13]. The obtained specific surface area varied from 34.25 to 42.70 m^2/g, which was smaller compared to that in the present work.

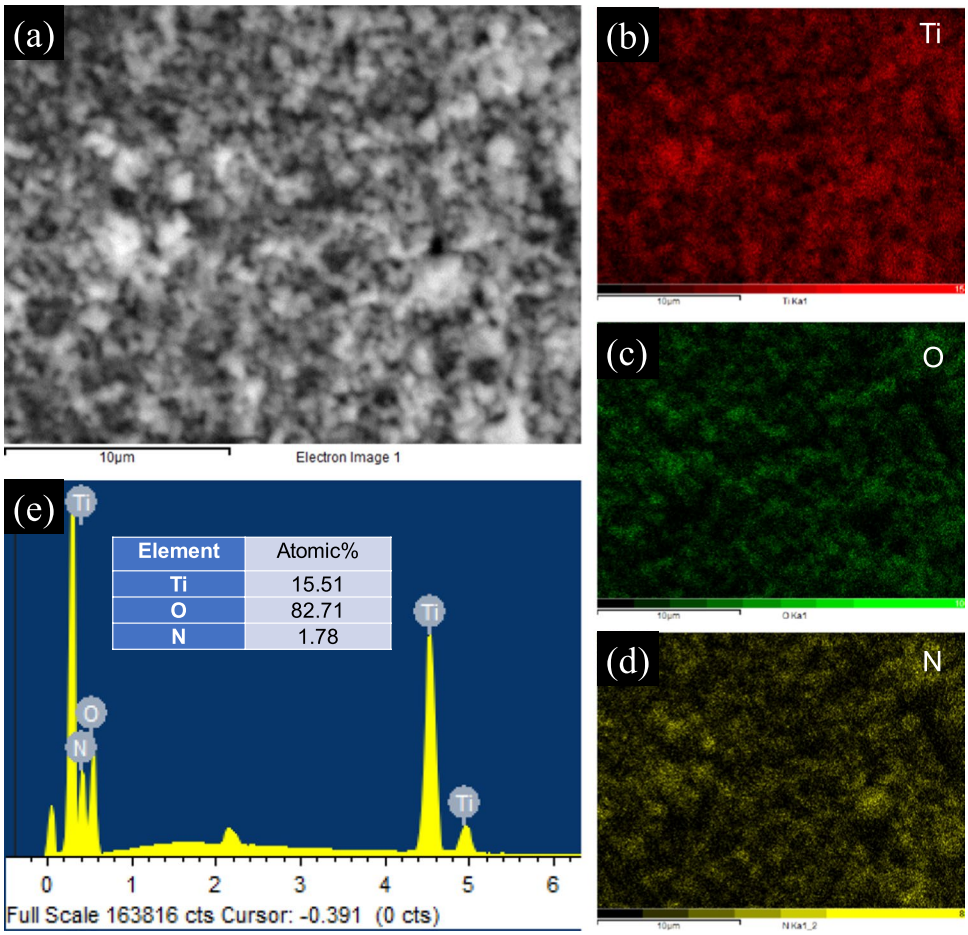

Fig. 6 **a–d** Elemental mapping images, and **e** EDX spectrum of 6-N-TiO_2

Photocatalytic activity

To evaluate the photocatalytic activity of N-TiO_2, colorless and colored model pollutants such as SA (drug), MB, and RhB (model dyes) were utilized in this experiment. Generally, when TiO_2 is irradiated by visible light, electron–hole pairs are generated on the valence and conduction band. These charge carriers can recombine each other producing heat [42, 43]. However, this electron–hole recombination could be suppressed by N doping to localize new level energy in N 2p orbitals and then narrow the band-gap energy. In addition, N doping also enabled the photogeneration of additional electron–hole pairs, thereby enhancing the photocatalytic activity [8]. Furthermore, the excited electrons in the conduction band react with adsorbed oxygen to form superoxide radicals ($O_2^{\bullet-}$), and holes in the valence band interact with H_2O or OH^- to produce hydroxyl radicals ($OH^{\bullet}$). Subsequently, these ROS ($O_2^{\bullet-} + OH^{\bullet}$) attack the model pollutants for degradation and mineralization process [44–47]. The details of photocatalytic reactions are illustrated in Equation R1-R6 and Fig. 9.

$$\mathrm{N-TiO_2} + h\nu \rightarrow \mathrm{N-TiO_2}\left(h^+ + e^-\right) \quad \text{(R1)}$$

$$\mathrm{N-TiO_2}\left(h^+ + e^-\right) \rightarrow \mathrm{N-TiO_2} + \text{heat} \quad \text{(R2)}$$

$$e^- + \mathrm{O_2} \rightarrow \mathrm{O_2^{\bullet-}} \quad \text{(R3)}$$

$$h^+ + \mathrm{H_2O} \rightarrow \mathrm{OH^{\bullet}} + H^+ \quad \text{(R4)}$$

$$h^+ + \mathrm{OH\text{-}^-} \rightarrow \mathrm{OH^{\bullet}} \quad \text{(R5)}$$

$$\text{ROS } (\mathrm{O_2^{\bullet-}} + \mathrm{OH^{\bullet}}) + \text{model pollutant} \rightarrow \text{degradation} \quad \text{(R6)}$$

Figure 10a exhibits the degradation percentage of colorless SA under visible irradiation for 50 min. In general, no degradation was found during the irradiation of SA without a catalyst (photolysis). In the presence of catalyst and light, pure TiO_2 showed photocatalytic activity during the reaction, but it was lower compared to all N-TiO_2 samples. Then, the photocatalytic activity was evaluated depending on N

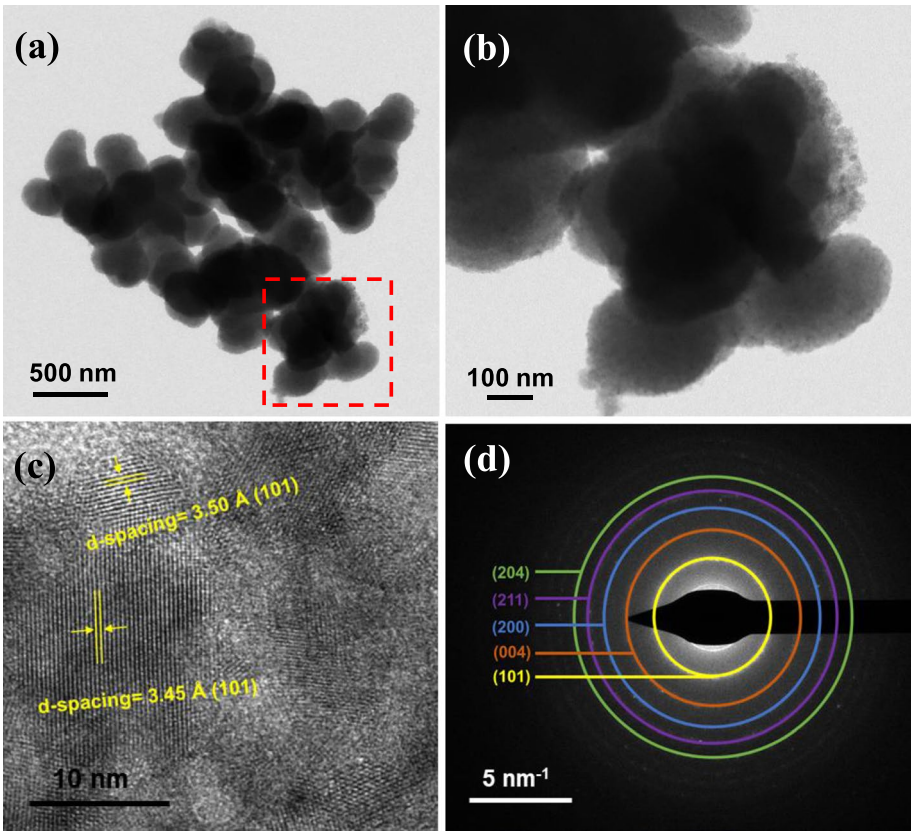

Fig. 7 **a**, **b** TEM images **c** HR-TEM, and **d** SAED pattern of 2-N-TiO_2 photocatalyst

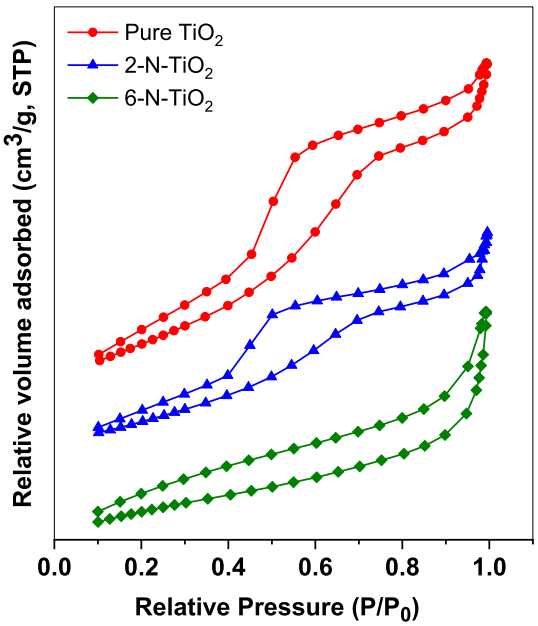

Fig. 8 Nitrogen adsorption–desorption isotherms of pure TiO_2 and N-TiO_2

Table 2 Surface area and porosity parameters of pure TiO_2 and N-TiO_2 samples

Sample	Multi-point BET	BJH desorption	
	Surface area (m^2/g)	Average pore volume (cm^3/g)	Average pore diameter (nm)
Pure TiO_2	95.907	0.161	1.927
2-N-TiO_2	67.841	0.106	1.703
6-N-TiO_2	63.743	0.083	1.692

concentration to select the most efficient one. The results showed that 2-N-TiO_2 (74.1%) exhibited the optimum degradation of SA compared to 4-N-TiO_2 (65.5%) and 6-N-TiO_2 (49.1%).

Additionally, the pseudo-first-order kinetic reaction also exhibited a similar tendency in which 2-N-TiO_2 performed a faster degradation than 4-N-TiO_2 and 6-N-TiO_2 (Fig. 10b). The reaction rate constants of 2-N-TiO_2, 4-N-TiO_2, and 6-N-TiO_2 were 0.0265, 0.0185, and 0.0124 min^{-1}, respectively (Table 3). The decrease of photocatalytic activity at higher nitrogen concentrations could be explained by the fact that the excessive nitrogen dopants could produce larger aggregated particles, cover the mesoporous structure then obstruct the pore and active sites, which promoted a decrease in the photocatalytic performance [48]. This is in accordance with

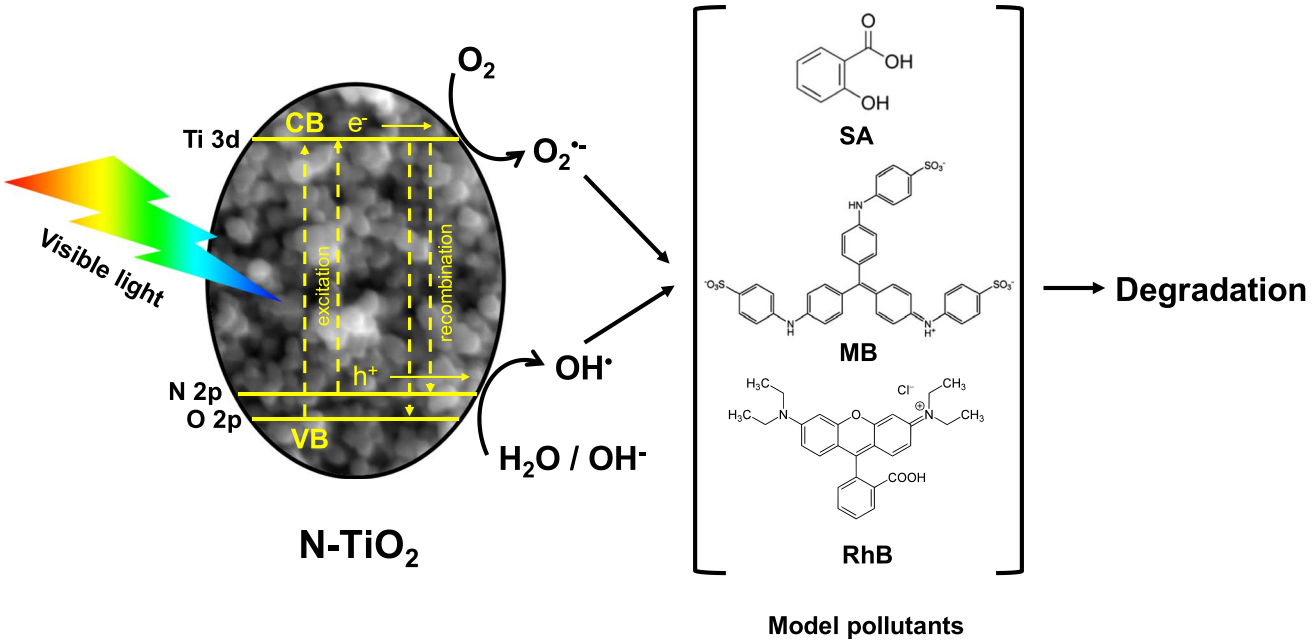

Fig. 9 Schematic photocatalytic reaction for the degradation of model pollutants over N-TiO_2 under visible light irradiation

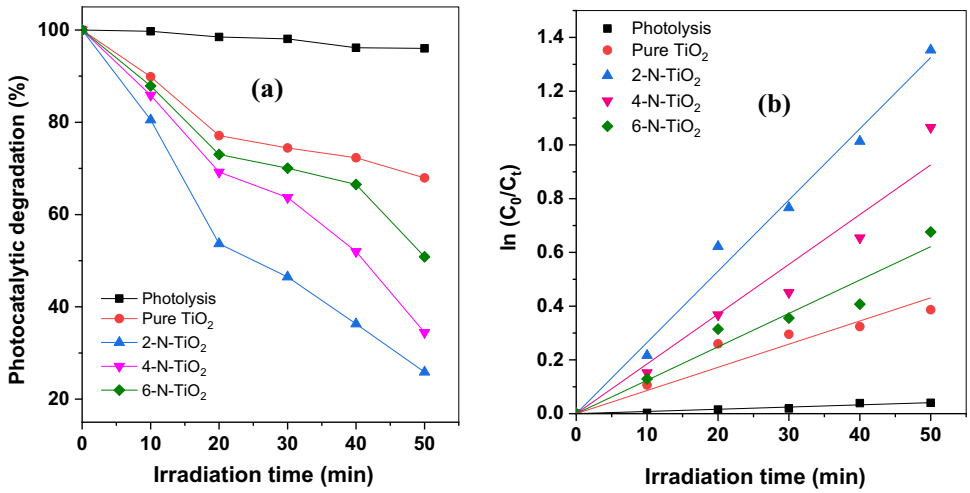

Fig. 10 **a** Photocatalytic degradation and **b** pseudo first-order kinetic reaction of SA over pure TiO_2 and N-TiO_2

Table 3 Photocatalytic degradation rate constant (k) and R^2 regression of different model pollutants over photocatalysts

Photocatalyst	Degradation rate constant, k (min^{-1})			R^2		
	SA	MB	RhB	SA	MB	RhB
Pure TiO_2	0.00862	0.00678	0.03682	0.96631	0.96531	0.99790
2-N-TiO_2	0.02651	0.01806	0.10711	0.99548	0.93526	0.99496
4-N-TiO_2	0.01852	0.01636	0.08408	0.97575	0.97243	0.99469
6-N-TiO_2	0.01243	0.01299	0.01858	0.97826	0.92398	0.9941

the BET results where the specific surface area of 6-N-TiO_2 (63.743 m^2/g) was lower than 2-N-TiO_2 (67.841 m^2/g). In addition, decreasing the crystalline structure of TiO_2 after N doping at higher concentrations as discussed in the XRD analysis could be another factor to reduce the photocatalytic activity. Higher crystalline structure could enhance the light-harvesting which is critical in the photocatalytic activity of N-TiO_2 [13, 19].

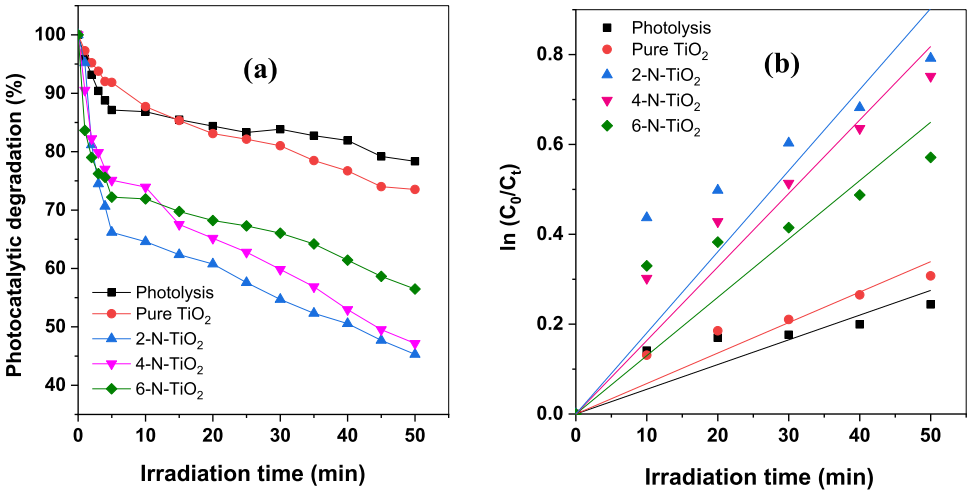

Fig. 11 **a** Photocatalytic degradation and **b** pseudo first-order kinetic reaction of MB over pure TiO_2 and N-TiO_2

Furthermore, the colored pollutants such as MB and RhB were used to evaluate the photocatalytic activity of prepared catalysts. Figure 11a shows the photocatalytic degradation of MB over pure TiO_2 and N-TiO_2 under visible irradiation. An identical tendency with that of the SA was shown, where 2-N-TiO_2 had an optimum photocatalytic activity compared with other samples. According to the results, 2-N-TiO_2 could decompose the MB sample with approximately 54.7%, followed by 4-N-TiO_2 (52.8%), 6-N-TiO_2 (43.5%), and pure TiO_2 (26.4%) for 50 min irradiation time. The reaction rate constant of 2-N-TiO_2, 4-N-TiO_2, and 6-N-TiO_2 for MB degradation were 0.0180, 0.0163, and 0.0129 min^{-1}, respectively (Fig. 11b and Table 3).

Figure 12a represents the photocatalytic activity of prepared samples toward RhB degradation under visible irradiation. Similar to the cases of MB, 2-N-TiO_2 showed an optimum RhB degradation compared to other samples. The degradation percentage of 2-N-TiO_2, 4-N-TiO_2, 6-N-TiO_2, and pure TiO_2 after 22 min irradiation were 90.4, 84.8, 33.0, and 54.7%, respectively. The degradation rate constants of RhB were 0.1071, 0.0840, 0.0185, and 0.0368 min^{-1} over 2-N-TiO_2, 4-N-TiO_2, 6-N-TiO_2, and pure TiO_2, respectively (Fig. 12b and Table 3). A different tendency was found for 6-N-TiO_2 which was lower than pure TiO_2. It might be due to a low crystallite size of 6-N-TiO_2 and affecting to adsorption process of RhB and then photocatalytic activity [19].

General photo-degradation pathways of RhB were reported by Zhang and fellow workers [49]. The reactive oxygen species, ROS ($O_2^{\bullet-} + OH^{\bullet}$) generated in the photocatalytic reaction played a major role in the degradation of RhB. The initial process was the formation of the N-deethylated of RhB. After N-deethylation, the pathways were more complex by ring-opening resulting in the formation of small molecules [49].

Subsequently, among the three different organic model pollutants, RhB performed the highest degradation efficiency over 2-N-TiO_2, compared to SA and MB as shown in Fig. 13. The reaction rate constant of 2-N-TiO_2 over RhB,

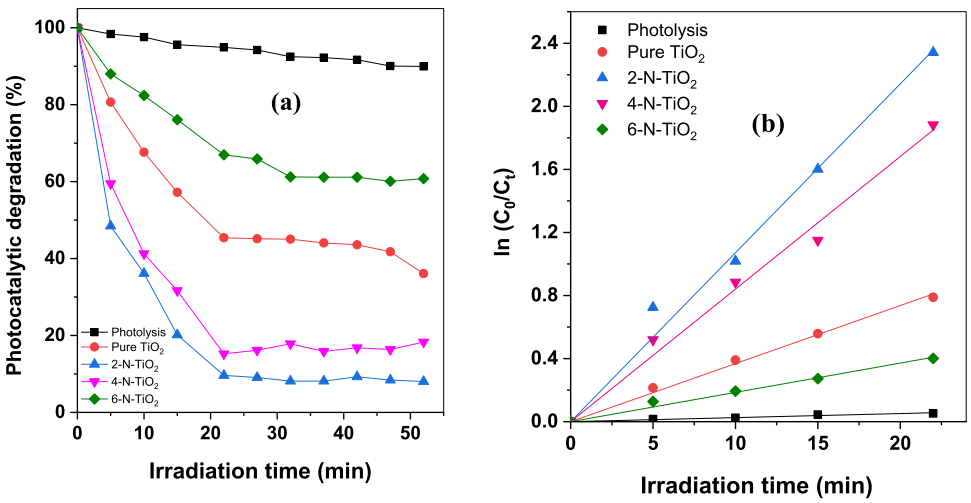

Fig. 12 **a** Photocatalytic degradation and **b** pseudo first-order kinetic reaction of RhB over pure TiO_2 and N-TiO_2

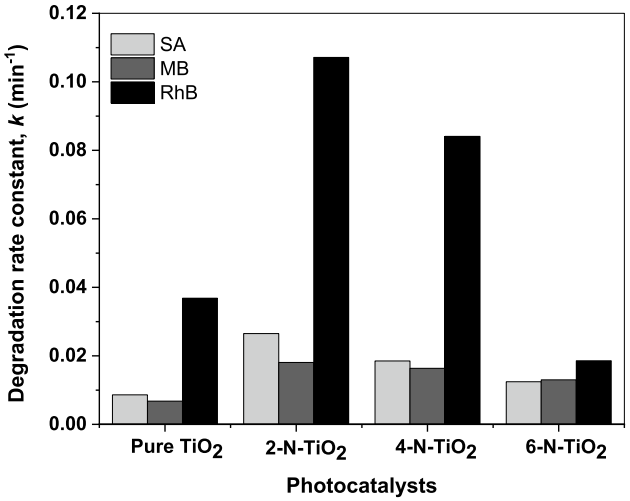

Fig. 13 Comparison of degradation rate constants of various model pollutants over prepared photocatalysts

SA, and MB were 0.1071, 0.0265, and 0.0180 min^{-1}, respectively. It could be assigned to different adsorption capacities of the catalysts which then affecting the photocatalytic activity [50]. Pal and co-workers compared the photocatalytic degradation of RhB, methylene blue, and 4-nitrophenol over standard Degussa P25 TiO_2 [50]. The degradation efficiency of RhB showed the highest one compared to other pollutants. The apparent reaction rate constant of RhB, methylene blue, and 4-nitrophenol were 0.045, 0.023, and 0.008 min^{-1}, respectively. Therefore, it is noteworthy that selecting an appropriate organic model pollutant is also a crucial parameter of the photocatalytic activity of the catalyst.

Conclusion

Herein, we report the successful synthesis of N-TiO_2 photocatalysts using urea as the nitrogen source and ethanol as a single solvent through the sol–gel method at ambient temperature and pressure. The concentration of urea affected the crystalline phase and size. The pure TiO_2, 2-N-TiO_2, and 4-N-TiO_2 samples showed high purity of anatase. However, the crystalline phase transformed into amorphous at higher urea concentration (6-N-TiO_2). In addition, the crystallite size decreased when increasing urea concentration. The prepared N-TiO_2 displayed a nano-spherical shape with an aggregation. The band-gap energy of N–TiO_2 was slightly lower than pure TiO_2, indicating that nitrogen doping could enhance the visible-light absorption of TiO_2. The photocatalytic experiments under visible irradiation showed that 2-N-TiO_2 had an optimum photocatalytic degradation performance compared to other samples. The photocatalytic degradation rate constant of RhB, SA, and MB were 0.1071, 0.0265, and 0.0180 min^{-1}, respectively. From this point of view, apart from developing an efficient, facile, and cost-effective synthesis route, it is also critical to select a proper model pollutant to obtain an optimum photocatalytic performance of 2-N-TiO_2.

Supplementary Information The online version contains supplementary material available at https://doi.org/10.1007/s11243-024-00584-9.

Acknowledgements This work was funded by "Net Zero Emission-BRIN" program with contract number of 1567/II.7/HK.01.00/3/2023; and also funded by "Program Riset dan Inovasi untuk Indonesia Maju Gelombang 3" with contract number of 12/II.7/HK/2023; and supported by the Ministry for Innovation and Technology of Hungary from the National Research, Development and Innovation Fund, financed under the 2021 Thematic Excellence Program funding scheme with a grant number TKP2021-NKTA-21.

Author contributions AW contributed to conceptualization, data curation, formal analysis, methodology, investigation, visualization, and writing—original draft. LR contributed to methodology, investigation, data curation and visualization. GET contributed to conceptualization, data curation, funding acquisition, supervision, validation, and writing—review and editing. DA contributed to validation, and writing—review and editing. DSK contributed to validation, and writing—review and editing. ND contributed to validation, and writing—review and editing. NY contributed to data curation and investigation. E.S.-B contributed to validation, and writing—review and editing, supervision. OH contributed to validation, and writing—review and editing, supervision. MMK contributed to validation, and writing—review and editing, supervision.

Data availability All the data are shown in the manuscript and supplementary information.

Declarations

Conflict of interest The authors have no competing interests to declare that are relevant to the content of this article.

References

1. Rueda-Marquez JJ, Levchuk I, Fernández Ibañez P, Sillanpää M (2020) A critical review on application of photocatalysis for toxicity reduction of real wastewaters. J Clean Prod 258:120694. https://doi.org/10.1016/j.jclepro.2020.120694
2. Wang JL, Xu LJ (2012) Advanced oxidation processes for wastewater treatment: formation of hydroxyl radical and application. Crit Rev Environ Sci Technol 42:251–325. https://doi.org/10.1080/10643389.2010.507698
3. Nobre FX, Gil Pessoa WA, Ruiz YL et al (2019) Facile synthesis of nTiO_2 phase mixture: characterization and catalytic performance. Mater Res Bull 109:60–71. https://doi.org/10.1016/j.materresbull.2018.09.019
4. Mangala KJ (2023) Green synthesis of titanium dioxide nanoparticles using Thymus vulgaris leaf extract for biological applications. Adv Nat Sci Nanosci Nanotechnol 14:35016. https://doi.org/10.1088/2043-6262/acf2ed
5. Khan MM, Ansari SA, Pradhan D et al (2014) Band gap engineered TiO_2 nanoparticles for visible light induced photoelectrochemical and photocatalytic studies. J Mater Chem A 2:637–644. https://doi.org/10.1039/c3ta14052k

6. Natarajan TS, Mozhiarasi V, Tayade RJ (2021) Nitrogen doped titanium dioxide (N-TiO_2): synopsis of synthesis methodologies, doping mechanisms, property evaluation and visible light photocatalytic applications. Photochem 1:371–410. https://doi.org/10.3390/photochem1030024
7. Ancy K, Sarojini V, Christy AJ et al (2022) Antibacterial activities and photocatalyzed degradation of textile dyeing waste water by Mn and F co-doped TiO_2 nanoparticles. Adv Nat Sci Nanosci Nanotechnol 13:45005. https://doi.org/10.1088/2043-6262/ac9c53
8. Asahi R, Morikawa T, Irie H, Ohwaki T (2014) Nitrogen-doped titanium dioxide as visible-light-sensitive photocatalyst: designs, developments, and prospects. Chem Rev 114:9824–9852. https://doi.org/10.1021/cr5000738
9. Ansari SA, Khan MM, Ansari MO, Cho MH (2016) Nitrogen-doped titanium dioxide (N-doped TiO_2) for visible light photocatalysis. New J Chem 40:3000–3009. https://doi.org/10.1039/C5NJ03478G
10. Calisir MD, Gungor M, Demir A et al (2020) Nitrogen-doped TiO_2 fibers for visible-light-induced photocatalytic activities. Ceram Int 46:16743–16753. https://doi.org/10.1016/j.ceramint.2020.03.250
11. Suwannaruang T, Kamonsuangkasem K, Kidkhunthod P et al (2018) Influence of nitrogen content levels on structural properties and photocatalytic activities of nanorice-like N-doped TiO_2 with various calcination temperatures. Mater Res Bull 105:265–276. https://doi.org/10.1016/j.materresbull.2018.05.010
12. Khalili V, Khalil-Allafi J, Maleki-Ghaleh H (2013) Titanium oxide (TiO_2) coatings on NiTi shape memory substrate using electrophoretic deposition process. Int J Eng Trans A Basics 26:707–712. https://doi.org/10.5829/idosi.ije.2013.26.07a.05
13. Suwannaruang T, Kidkhunthod P, Chanlek N et al (2019) High anatase purity of nitrogen-doped TiO_2 nanorice particles for the photocatalytic treatment activity of pharmaceutical wastewater. Appl Surf Sci 478:1–14. https://doi.org/10.1016/j.apsusc.2019.01.158
14. Sanchez-Martinez A, Ceballos-Sanchez O, Koop-Santa C et al (2018) N-doped TiO_2 nanoparticles obtained by a facile coprecipitation method at low temperature. Ceram Int 44:5273–5283. https://doi.org/10.1016/j.ceramint.2017.12.140
15. Marques J, Gomes TD, Forte MA et al (2019) A new route for the synthesis of highly-active N-doped TiO_2 nanoparticles for visible light photocatalysis using urea as nitrogen precursor. Catal Today. https://doi.org/10.1016/j.cattod.2018.09.002
16. Wafi A, Szabó-Bárdos E, Horváth O et al (2021) Coumarin-based quantification of hydroxyl radicals and other reactive species generated on excited nitrogen-doped TiO_2. J Photochem Photobiol A Chem 404:112913. https://doi.org/10.1016/j.jphotochem.2020.112913
17. Hu Y, Liu H, Kong X, Guo X (2014) Effect of calcination on the visible light photocatalytic activity of N-doped TiO_2 prepared by the sol-gel method. J Nanosci Nanotechnol 14:3532–3537. https://doi.org/10.1166/jnn.2014.8021
18. Khan JA, Sayed M, Shah NS et al (2023) Synthesis of N-doped TiO_2 nanoparticles with enhanced photocatalytic activity for 2,4-dichlorophenol degradation and H2 production. J Environ Chem Eng 11:111308. https://doi.org/10.1016/j.jece.2023.111308
19. Mahendrasingh P, Vrushali N, Manisha G et al (2020) Effect of nitrogen doping on photocatalytic activity of TiO_2. J Nanosci Technol 6:918–923. https://doi.org/10.30799/jnst.312.20060401
20. Zhang T, Sun L, Liu R et al (2012) A novel naturally occurring salicylic acid analogue acts as an anti-inflammatory agent by inhibiting nuclear factor-kappaB activity in RAW264.7 macrophages. Mol Pharm 9:671–677. https://doi.org/10.1021/mp2003779
21. Kaur H, Kaur R (2014) Removal of Rhodamine-B dye from aqueous solution onto Pigeon dropping: adsorption, kinetic, equilibrium and thermodynamic studies. J Mater Environ Sci 5:1830–1838
22. Wafi A, Szabó-Bárdos E, Horváth O et al (2020) The photocatalytic and antibacterial performance of nitrogen-doped TiO_2: surface-structure dependence and silver-deposition effect. Nanomaterials 10:2261. https://doi.org/10.3390/nano10112261
23. Chung WJ, Nguyen DD, Bui XT et al (2018) A magnetically separable and recyclable Ag-supported magnetic TiO_2 composite catalyst: fabrication, characterization, and photocatalytic activity. J Environ Manage 213:541–548. https://doi.org/10.1016/j.jenvman.2018.02.064
24. Asadzadeh Patehkhor H, Fattahi M, Khosravi-Nikou M (2021) Synthesis and characterization of ternary chitosan–TiO_2–ZnO over graphene for photocatalytic degradation of tetracycline from pharmaceutical wastewater. Sci Rep 11:24177. https://doi.org/10.1038/s41598-021-03492-5
25. Xia Z, Xing S, Wang H et al (2022) Weak-visible-light-driven Fe doped TiO_2 photocatalyst prepared by coprecipitation method and degradation of methyl orange. Opt Mater (Amst) 129:112522. https://doi.org/10.1016/j.optmat.2022.112522
26. Yu JG, Yu HG, Cheng B et al (2003) The effect of calcination temperature on the surface microstructure and photocatalytic activity of TiO_2 thin films prepared by liquid phase deposition. J Phys Chem B 107:13871–13879. https://doi.org/10.1021/jp036158y
27. Cheng J, Chen J, Lin W et al (2015) Improved visible light photocatalytic activity of fluorine and nitrogen co-doped TiO_2 with tunable nanoparticle size. Appl Surf Sci 332:573–580. https://doi.org/10.1016/J.APSUSC.2015.01.218
28. Cheng X, Yu X, Xing Z, Yang L (2016) Synthesis and characterization of N-doped TiO_2 and its enhanced visible-light photocatalytic activity. Arab J Chem 9:S1706–S1711. https://doi.org/10.1016/j.arabjc.2012.04.052
29. Li Y, Jiang Y, Peng S, Jiang F (2010) Nitrogen-doped TiO_2 modified with NH4F for efficient photocatalytic degradation of formaldehyde under blue light-emitting diodes. J Hazard Mater 182:90–96. https://doi.org/10.1016/J.JHAZMAT.2010.06.002
30. Kim HK, Roh JS, Choi DJ (2010) Crystallization behavior caused by N doping in $Ge_1Sb_4Te_7$ for PCRAM application. Thin Solid Films 518:6422–6428. https://doi.org/10.1016/j.tsf.2010.02.002
31. Shehata MA, Shama SA, Mahmoud SA, Doheim MM (2016) Preparation and characterization of various interstitial N-Doped TiO_2 catalysts from different nitrogen dopants for the treatment of polluted water. Chem Mater Res 8:45–55
32. Vaiano V, Sacco O, Sannino D, Ciambelli P (2015) Nanostructured N-doped TiO_2 coated on glass spheres for the photocatalytic removal of organic dyes under UV or visible light irradiation. Appl Catal B Environ 170–171:153–161. https://doi.org/10.1016/j.apcatb.2015.01.039
33. Batzill M, Morales EH, Diebold U (2006) Influence of nitrogen doping on the defect formation and surface properties of TiO_2 rutile and anatase. Phys Rev Lett. https://doi.org/10.1103/PhysRevLett.96.026103
34. Yang G, Jiang Z, Shi H et al (2010) Preparation of highly visible-light active N-doped TiO_2 photocatalyst. J Mater Chem 20:5301–5309. https://doi.org/10.1039/c0jm00376j
35. Samsudin EM, Abd Hamid SB, Juan JC et al (2015) Controlled nitrogen insertion in titanium dioxide for optimal photocatalytic degradation of atrazine. RSC Adv 5:44041–44052. https://doi.org/10.1039/c5ra00890e
36. Leyva-Porras C, Toxqui-Teran A, Vega-Becerra O et al (2015) Low-temperature synthesis and characterization of anatase TiO_2 nanoparticles by an acid assisted sol-gel method. J Alloys Compd 647:627–636. https://doi.org/10.1016/j.jallcom.2015.06.041
37. Wang G, Xu L, Zhang J et al (2012) Enhanced photocatalytic activity of TiO_2 powders (P25) via calcination treatment. Int J Photoenergy 2012:1–9. https://doi.org/10.1155/2012/265760

38. Ma J, Chu J, Qiang L, Xue J (2013) Effect of different calcination temperatures on the structural and photocatalytic performance of Bi-TiO_2/SBA-15. Int J Photoenergy 2013:1–11. https://doi.org/10.1155/2013/875456
39. Yu J, Yu JC, Cheng B, Zhao X (2003) Preparation and characterization of highly photoactive nanocrystalline TiO2 powders by solvent evaporation-induced crystallization method. Sci China Ser B Chem 46:549–557. https://doi.org/10.1360/03YB0012/METRICS
40. Sing KSW, Everett DH, Haul RAW et al (1985) Reporting Physisorption data for gas/solid systems with special reference to the determination of surface area and porosity. Pure Appl Chem 57:603–619. https://doi.org/10.1351/PAC198557040603/MACHINEREADABLECITATION/RIS
41. Ayinla RT, Dennis JO, Zaid HM et al (2019) A review of technical advances of recent palm bio-waste conversion to activated carbon for energy storage. J Clean Prod 229:1427–1442. https://doi.org/10.1016/j.jclepro.2019.04.116
42. Khan MM (2023) Theoretical concepts of photocatalysis. Elsevier, Netherlands. https://doi.org/10.1016/C2021-0-01798-3
43. Khan MM, Pradhan D, Sohn Y (2017) Springer series on polymer and composite materials. Nanocomposites for visible light-induced photocatalysis. Springer, Cham, Switzerland, pp 1–200. https://doi.org/10.1007/978-3-319-62446-4
44. Dong S, Feng J, Fan M et al (2015) Recent developments in heterogeneous photocatalytic water treatment using visible light-responsive photocatalysts: a review. RSC Adv 5:14610–14630. https://doi.org/10.1039/c4ra13734e
45. Kisch H (2013) Semiconductor photocatalysis - Mechanistic and synthetic aspects. Angew Chem Int Ed 52:812–847. https://doi.org/10.1002/anie.201201200
46. Zhu X, Zhou Q, Xia Y et al (2021) Preparation and characterization of Cu-doped TiO_2 nanomaterials with anatase/rutile/brookite triphasic structure and their photocatalytic activity. J Mater Sci Mater Electron 32:21511–21524. https://doi.org/10.1007/s10854-021-06660-5
47. Zhu X, Wang J, Yang D et al (2021) Fabrication, characterization and high photocatalytic activity of Ag-ZnO heterojunctions under UV-visible light. RSC Adv 11:27257–27266. https://doi.org/10.1039/d1ra05060e
48. Mohtar SS, Aziz F, Ismail AF et al (2021) Impact of doping and additive applications on photocatalyst textural properties in removing organic pollutants: a review. Catalysts 11:1160
49. Zhang Y, Zhou J, Li Z, Feng Q (2018) Photodegradation pathway of rhodamine B with novel Au nanorods @ ZnO microspheres driven by visible light irradiation. J Mater Sci 53:3149–3162. https://doi.org/10.1007/s10853-017-1779-x
50. Pal S, Taurino A, Catalano M, Licciulli A (2022) Block copolymer and cellulose templated mesoporous TiO_2-SiO_2 nanocomposite as superior photocatalyst. Catalysts 12:770. https://doi.org/10.3390/catal12070770

Authors and Affiliations

Abdul Wafi[1,2] · Liszulfah Roza[3] · Gerald Ensang Timuda[3] · Demas Aji[1] · Deni Shidqi Khaerudini[1] · Nono Darsono[4] · Nurfina Yudasari[5] · Erzsébet Szabó-Bárdos[6] · Ottó Horváth[6] · Mohammad Mansoob Khan[7]

✉ Abdul Wafi
abdul.wafi.1@brin.go.id

Liszulfah Roza
lisz001@brin.go.id

Gerald Ensang Timuda
gerald.ensang.timuda@brin.go.id

Demas Aji
demas.aji@hotmail.com

Deni Shidqi Khaerudini
deni.shidqi.khaerudini@brin.go.id

Nono Darsono
nono.darsono@brin.go.id

Nurfina Yudasari
nurfina.yudasari@brin.go.id

Erzsébet Szabó-Bárdos
szabone.bardos.erzsebet@mk.uni-pannon.hu

Ottó Horváth
horvath.otto@mk.uni-pannon.hu

Mohammad Mansoob Khan
mansoob.khan@ubd.edu.bn

[1] Research Center for Advanced Materials, National Research and Innovation Agency (BRIN), South Tangerang, Indonesia

[2] Department of Pharmacy, Faculty of Medicine and Health Science, Universitas Islam Negeri Maulana Malik Ibrahim, Malang, Indonesia

[3] Research Center for Nanotechnology Systems, National Research and Innovation Agency (BRIN), South Tangerang, Indonesia

[4] Research Center for Energy Conversion and Conservation, National Research and Innovation Agency (BRIN), South Tangerang, Indonesia

[5] Research Center for Photonics, National Research and Innovation Agency (BRIN), South Tangerang, Indonesia

[6] Research Group of Environmental and Inorganic Photochemistry, Center for Natural Sciences, University of Pannonia, Veszprém, Hungary

[7] Chemical Sciences, Faculty of Science, Universiti Brunei Darussalam, Jalan Tungku Link, Gadong BE1410, Brunei Darussalam